A New Efficient Thermomechanical Reliability Model for Lead-Free Solder Joints

Jean-Baptiste Libot and Philippe Milesi
Hooke Electronics

ABSTRACT

The thermomechanical reliability of solder joints remains a challenge for companies whose electronic equipment is used in harsh thermal conditions throughout their lifecycle, such as in the aeronautics, space, military or medical applications. With the RoHS legislation and REACh directive preventing lead from being used in electronic equipment, 96.5Sn-3.0Ag-0.5Cu (SAC305) composition has become one of the most widely used lead-free solder alloys. Various models are available to evaluate the reliability of solder joints under temperature cycles, ranging from simple analytical models to complex Finite Element Analysis (FEA). While analytical models are easy-to-use, they may lack the precision needed for accurate lifetime assessments. Conversely, FEA, though more precise, requires expertise, is time-consuming, and may not be cost-efficient.

This study aims to present a new analytical model that accounts for the shape of solder joints, with a special emphasis on the determination of the mechanical properties of the Printed Circuit Boards (PCBs) and components. A simplified elastic-plastic constitutive relationship coupled with a viscoplastic model is used to describe the behavior of SAC305 solder joints under temperature cycling. The reliability model presented in this study is calibrated and validated using over 100 durability data points from various leadless packages, PCB stack-ups, and thermal cycling conditions. It represents an efficient and easy-to-use tool for electronic designers to quickly and accurately evaluate the thermomechanical reliability of their electronic assemblies.

Key words: Lead-free, SAC305, thermal cycling, PCB, material characterization, solder joint reliability.

INTRODUCTION

The thermomechanical reliability of solder joints is a main concern for industries whose electronic assemblies used in the field are subjected to large temperature excursions. The Coefficient of Thermal Expansion (noted 'CTE' or 'α') mismatch between the components and the PCB leads to the cyclic shearing of the solder joints during thermal cycling, eventually resulting in electronic system failure due to solder joint thermomechanical fatigue. With the widespread adoption of SAC305 solder composition across the industry, numerous reliability models have been developed. Clech et al. conducted a review of existing solder joint life prediction models, including those addressing SAC305 alloy [1]. Empirical models, such as the Norris-Landzberg model initially developed for high-Pb content solders, have been adapted by several authors for SAC305 solder to calculate Acceleration Factors (AF) [2-4]. The review highlights that the constants of the Norris-Landzberg model depend on the electronic assemblies (packages and PCBs) used to derive the model, as well as the Accelerated Thermal Cycling (ATC) conditions. Therefore, extending its use to other Printed Circuit Board Assemblies (PCBAs) and ATC conditions is not recommended. The Engelmaier model, widely regarded as one of the most established in the solder joint reliability field, correlates the number of cycles to failure with the plastic strain range and has also been extended to SAC305 solder [5]. It is recognized that the model does not adequately account for solder joint geometry and does not handle the creep of solder joints accurately [6]. Moreover, the model involves a somewhat arbitrary calibration factor F accounting for second-order effects. Despite its limitations, the Engelmaier model remains widely used because it provides a direct and quick estimate of solder joint reliability. This demonstrates how electronic designers might prioritize the speed of their estimation over its accuracy and representativeness. To achieve a high level of representativeness in both the geometry and the constitutive models of the various materials in the PCBA, engineers can conduct FEA. Syed developed a fatigue model based on the evaluation of inelastic strain energy density accumulated in solder balls of Ball Grid Arrays (BGAs) and Chip Scale Packages (CSPs) for three harsh ATC conditions [7]. By using finite element analysis (FEA) and existing creep constitutive models for SAC solders, he correlated experimental durability data with the calculated inelastic strain energy density. His model exhibited a fatigue exponent of -1, which is close to the theoretical value predicted by the Palmgren-Miner rule for cyclic damage and consistent with findings from

another study on SAC305 Wafer-Level Packages (WLPs) [8]. Chai considered a similar approach to develop a fatigue model by calculating the inelastic strain energy density in a critical volume of Ceramic Leadless Chip Carrier (CLCC) solder joints, yielding a fatigue exponent of -2.6 [9]. This study covers a wide range of ATC conditions (nine) but only one type of electronic package, which limits its applicability. It is important to note that FEA requires specific skills from the user such as modeling and material characterization. Although FEA offers greater precision in terms of geometry and constitutive material equations compared to analytical reliability models, it is time-consuming, and non-linear simulations can take several hours to complete.

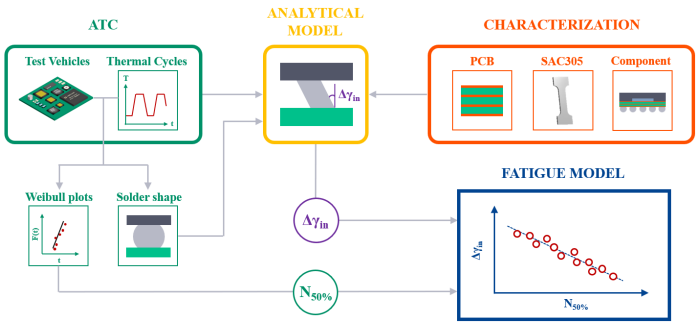

Figure 1: Overview of the methodology for developing an analytical thermomechanical reliability model for solder joints

This study aims to develop an analytical reliability model for SAC305 solder joints that addresses key limitations of existing models, such as the simplification of solder shape. Another objective of this study is to eliminate the need for any calibration factors. Test vehicles, consisting of three different packages (CLCCs, WLPs, and resistors), were reflow soldered with SAC305 solder alloy onto two different flame retardant (FR-4) PCBs, double-sided and multi-layered (8 copper layers) stack-up, with varying thicknesses. The test assemblies were then subjected to five different accelerated thermal cycling (ATC) conditions to determine the corresponding number of cycles to failure for a 50% failure rate ($N_{50\%}$) using a 2P-Weibull distribution. To develop an accurate thermomechanical reliability model, it is important to follow the steps outlined in Figure 1. Each element of the assembly must be carefully characterized to minimize errors in calculating the fatigue criteria and, ultimately, lifetime results. This includes measuring the Young's modulus and CTE of the components and PCB stack-up, as well as the elastic-plastic and viscoplastic mechanical properties of SAC305 solder alloy. In parallel with the solder joint reliability model development, complementary modules have been developed to evaluate the temperature-dependent mechanical properties of PCBs and multi-material components, such as BGAs. These mechanical properties are input data that must be accurately assessed to develop a robust reliability model. Finally, the resulting thermomechanical reliability model is validated using independent durability data.

EXPERIMENTAL WORK

Thermal cycling tests

Description of the test vehicles and setup

This study considered different daisy-chained components, including two types of Wafer Level Packages (WLPs): a 10×10 mm WLP400 and a 15×15 mm WLP900, both featuring a 0.3 mm ball diameter and a 0.5 mm pitch, soldered onto 0.3 mm diameter Non-Solder Mask Defined (NSMD) PCB pads , four types of Ceramic Leadless Chip Carriers (CLCC68, CLCC44, CLCC28 and CLCC20), three types of resistors (R2512, R2010 and R1210). Eight identical test vehicles are considered, and two sets of component types are assembled per board so that sixteen assemblies are investigated per configuration, allowing the statistical analysis of SAC305 solder joints durability. Each test vehicle depicts different PCB stack-ups and thicknesses:

- 0.8 mm Double Sided (DS) PCB,
- 1.6 mm Double Sided (DS) PCB,
- 3.2 mm Double Sided (DS) PCB,
- 1.6 mm Multi-Layer PCB with 8 Cu planes (ML8),

Figure 2 shows cross-sections of the 1.6 mm DS and ML8 boards, illustrating their corresponding stack-up. Each PCB presents a specific structure of glass cloth for the core and prepreg layers, therefore inducing specific material properties (CTE and Young's Modulus) for each test board (see section "Materials characterization").

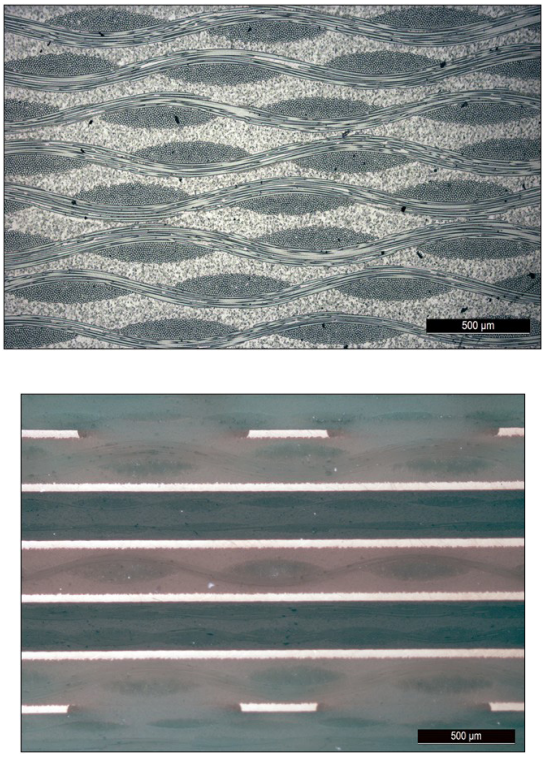

Figure 2: (a) DS and (b) ML8 PCB stack-up (the top and bottom Cu layers for each board are not visible)

Regardless of the PCB stack-up, the substrates are 220 × 220 mm FR-4 boards with Panasonic R1755V material. The boards have Electroless Nickel Immersion Gold (ENIG) surface finish on non-solder mask defined (NSMD) pads. Several Surface Mount Technology (SMT) components are mounted on the boards but only the WLP, CLCC and resistors are of interest in this study. Detachable test coupons are also designed for the failure analysis. The test vehicles considered in this study are representative of real assemblies manufactured in the industry as they were reflow soldered with SAC305 solder alloy as real boards are. Figure 3 shows the test assemblies with its corresponding detachable test coupon.

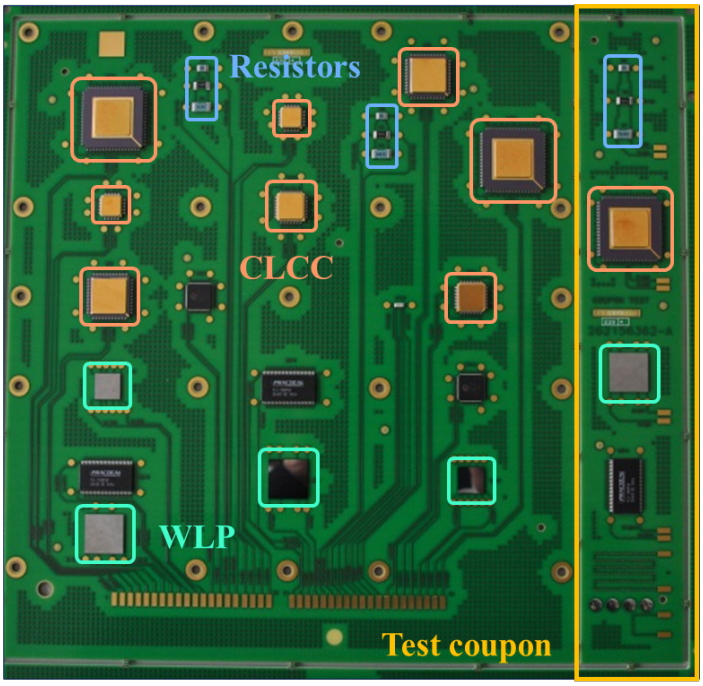

Figure 3: Test vehicle with CLCC, WLP and resistors packages

Test vehicles are then placed in a thermal chamber and connected to a data logger system allowing the continuous measurement of the electrical continuity. Except for the test coupons whose components resistance is checked out with a multimeter after removal from the thermal chamber, the daisy-chain resistance of each component is monitored throughout the thermal cycling test at the middle of each dwell time at low and high temperature in order to detect the number of cycles to failure. The failure criterion is based on the 20% increase in resistance for five consecutive scans according to the IPC-9701A standard [10]. As can be seen in figure 3, other SMT (Surface Mount Technology) components are soldered on the test vehicles. However, these were not considered in this study because no failure data were recorded by the end of the thermal cycling tests.

Temperature cycles and test matrix

Five different ATC conditions are tested to assess the influence of the temperature amplitude ΔT as well as the dwell time tD (a 10°C/min ramp rate is applied for each configuration). Table 1 presents the characteristics of each temperature cycle configuration.

Table 1: Temperature profiles

Thermal cycles:	Cycle 1	Cycle 2	Cycle 3	Cycle 4	Cycle 5
T_{min} (°C)	-55	-55	-55	-40	-20
T_{max} (°C)	125	125	125	85	65
tD (min)	15	30	120	15	15
dT/dt (°C.min^{-1})	10	10	10	10	10

Figure 4 graphically presents the temperature cycles applied for the different test vehicles. The ATC considered in this study cover a wide range of temperature amplitudes and dwell times.

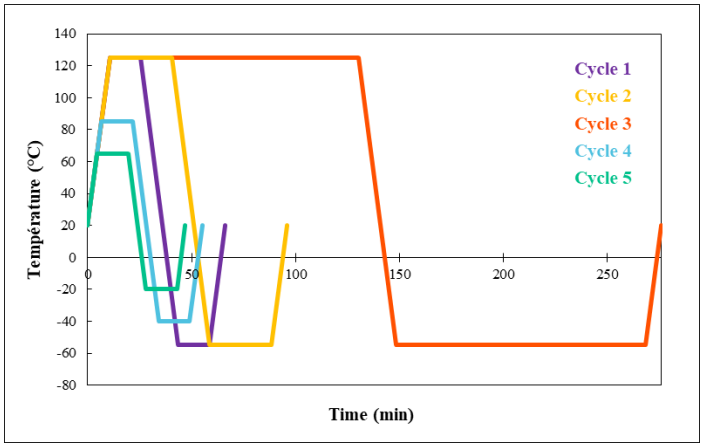

Figure 4: Temperature profiles

As mentioned previously, eight identical boards for each test vehicle configuration are considered in this study. As a result, since there are two identical components per board, sixteen failures can be recorded throughout the thermal cycling test for each component. The corresponding number of cycles to failure for a given failure rate ($N_{x\%}$) can then be determined using 2P-Weibull distribution. Table 2 presents the test matrix corresponding to the thermal cycling tests.

Table 2: Test matrix

PCB Stack-up	Cycle	PCB thickness	# of specimen
DS	Cycle 1	0.8 mm	16
		1.6 mm	16
		3.2 mm	16
	Cycle 2	1.6 mm	16
	Cycle 4	1.6 mm	16
	Cycle 1	0.8 mm	16
		1.6 mm	16
		3.2 mm	16
	Cycle 2	1.6 mm	16
	Cycle 4	1.6 mm	16
	Cycle 5	1.6 mm	16
ML8	Cycle 1	1.6 mm	16
	Cycle 2	1.6 mm	16
	Cycle 3	1.6 mm	16
	Cycle 4	1.6 mm	16
	Cycle 1	1.6 mm	16
	Cycle 2	1.6 mm	16
	Cycle 3	1.6 mm	16
	Cycle 4	1.6 mm	16

ATC results

Thermal cycling fatigue results are analyzed using the 2-parameter Weibull probability distribution, allowing the determination of the number of cycles to failure for any given failure probability:

$$F(t) = 1 - e^{-\left(\frac{t}{\eta}\right)^{\beta}}$$

Where F(t) is the cumulative failure distribution function or failure rate, η the characteristic life (number of cycles to failure for 63.2% of failed specimens), and β the shape parameter (characterizing the scatter in lifetime results). It is common to derive thermomechanical fatigue models considering $N_{50\%}$, i.e. for a failure probability of 50%. However, for critical applications such as equipment embedded in civil or military aircrafts, this failure probability is too important and one can rather refers to $N_{5\%}$ or even $N_{1\%}$ to derive thermomechanical durability models. Figure 5 shows the Weibull plots for the CLCC44 and WLP900 packages tested at various temperature amplitudes.

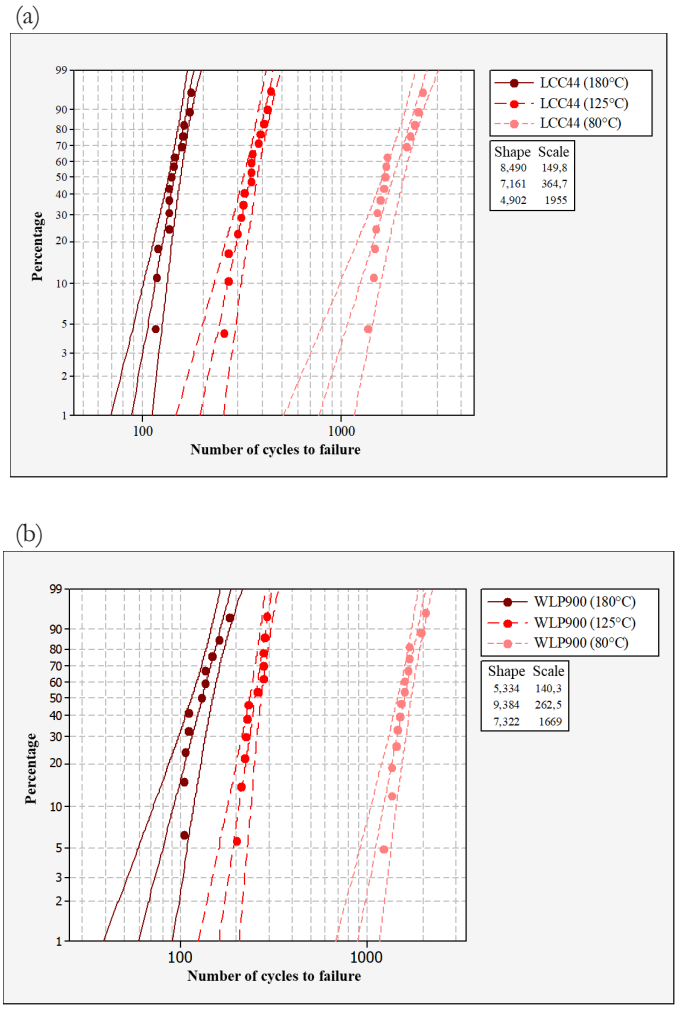

Figure 5: Influence of thermal amplitudes (80°C, 125°C, and 180°C). Weibull plots corresponding to (a) CLCC44 and (b) WLP900 packages.

The maximum thermal deformation generated at the critical solder joint is directly proportional to the temperature amplitude applied during accelerated temperature cycling tests. As a result, the thermomechanical damage of SAC305 solder joints increases with higher thermal excursions, leading to a reduced numbers of cycles to failure. Concerning the dwell times, it characterizes the stages of the cycle where thermal deformation at the solder joints remains constant. This parameter influences the mechanical behavior of the solder joints, as a longer dwell time allows for better stress relaxation compared to a shorter one. A basic assessment of the influence of dwell times was conducted by comparing the lifetime results ($N_{50\%}$) obtained from cycles 1, 2, and 3, corresponding to dwell times of 15, 30, and 120 minutes, respectively. Figure 6 is a graph illustrating the evolution of the number of cycles corresponding to a 50% probability of failure as a function of dwell times.

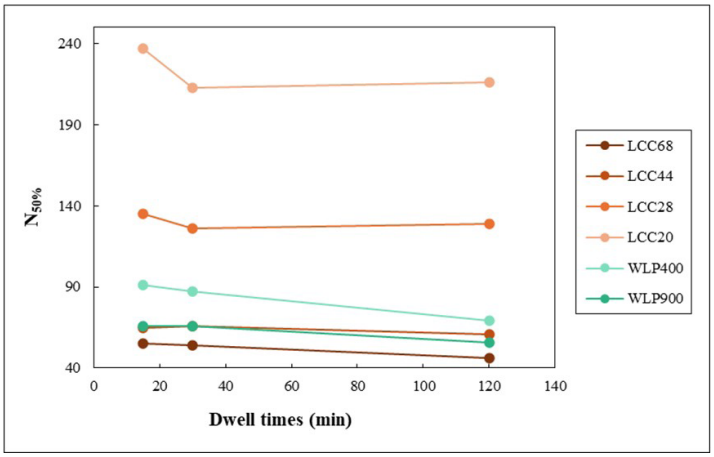

Figure 6: Evolution of the durability of CLCC and WLP packages as a function of dwell time

For very low durability results ($N_{50\%}$ < 100 cycles to failure), durability decreases as dwell time increases. For higher numbers of cycles to failure ($N_{50\%}$ > 100 cycles), durability tends to stabilize with increasing dwell time. The number of cycles to failure for the CLCC68, CLCC44, WLP900, and WLP400 packages is likely too low to highlight the asymptotic behavior of the durability results as dwell time increases. Although some resistors failed, when the thermal cycling test 3 was stopped, the resistors unfortunately did not exhibit enough failure to generate a Weibull plot.

MATERIALS CHARACTERIZATION

SAC305 solder alloy

Material characterization is a crucial step in developing a thermomechanical reliability model. Every element of the assembly must be thoroughly characterized to accurately estimate the fatigue criteria (solder joints inelastic shear strain 'Δγin' in this study). Monotonic tensile and stress relaxation tests were conducted using classic dog-bone samples to understand the thermomechanical behavior of the SAC305 solder alloy. Tensile tests were performed at different temperatures to simulate the various conditions encountered by real PCBAs in the field (-55°C, -40°C, 20°C, 85°C, and 125°C). The strain rate was set at $d\varepsilon/dt = 4.8\times10^{-5}\ s^{-1}$ to account for the very low strain rates involved during accelerated thermal cycling tests and in real applications. Figure 7 presents the obtained tensile stress-strain curves (three test samples were used for each configuration).

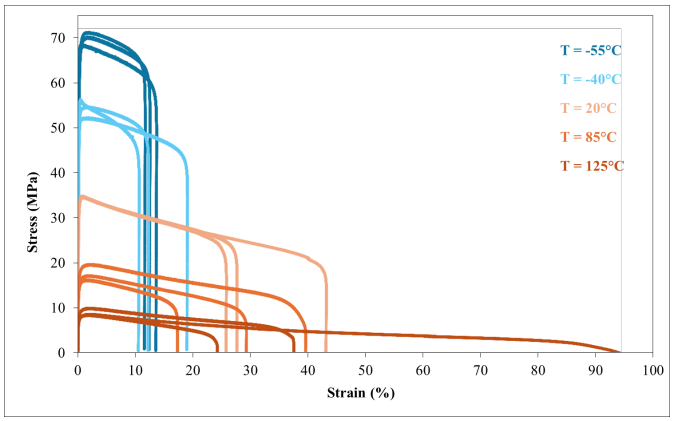

Figure 7: SAC305 stress-strain curves plotted at different temperatures

The higher the temperature, the lower the Ultimate Tensile Stress (UTS or 'σmax') and yield strength, and the higher the elongation at rupture. As temperature decreases, there is a progressive loss of ductility, but no ductile-to-brittle transition was observed within the temperature range considered in this study. Fracture surfaces were examined on samples tested at -55°C, 20°C, and 125°C. All samples exhibited 'dimples' typically observed in ductile fractures, which became larger as temperature increased. Figure 8 shows the fracture surface of a SAC305 sample tested at 20°C.

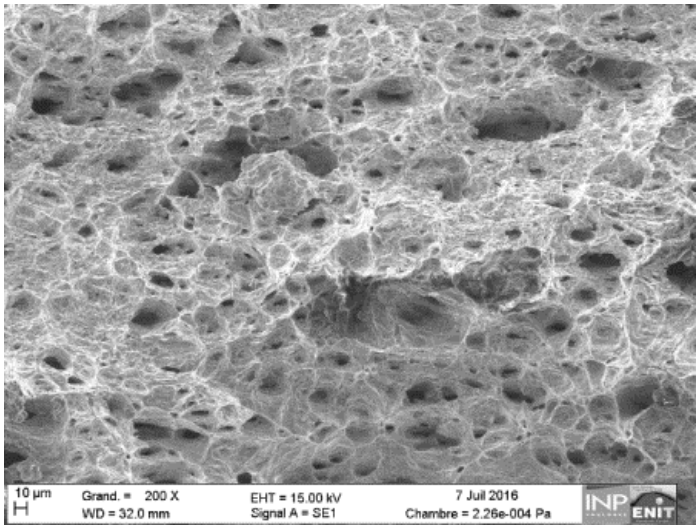

Figure 8: Fracture surface of a SAC305 specimen tested at 20°C

Observations of the fracture surfaces clearly indicate that plastic strains dominate the damage in the SAC305 alloy. From the tensile stress-strain data shown in Figure 5, it is possible to determine the Ultimate Tensile Stress (UTS) as a function of temperature. However, since solder joints undergoing temperature cycles are primarily subjected to shear loading, it is important to convert the maximum tensile stress into the maximum shear stress. Using the von Mises criterion, this can be expressed as follows:

$$\tau_{max} = \frac{\sigma_{max}}{\sqrt{3}}$$

Figure 9 shows the evolution of the maximum shear stress according to the temperature. Tensile data in the literature are scarce due to the geometry of the test specimens, the microstructure of the alloy, and intrinsic experimental setup parameters. Despite these discrepancies, the temperature-dependent maximum shear stresses obtained in this study are consistent with values reported in several publications [11-13].

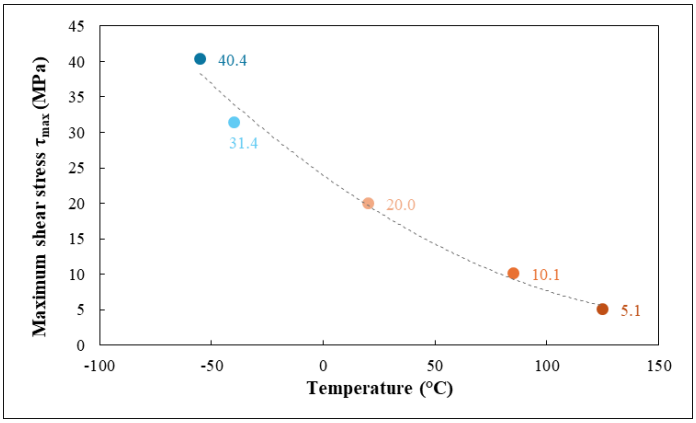

Figure 9: Evolution of the maximum shear stress as a function of temperature

Viscoplastic phenomena are believed to occur when $T_H = T/T_m > 0.4$ (T_H is the homologous temperature defined as the ratio between the temperature and the melting temperature of the material T_m) [14]. Between -55°C and 125°C (extrema temperatures for the considered thermal cycling conditions), SAC305 homologous temperatures are respectively close 0.45 and 0.80 (with a solidus temperature about 217°C for SAC305 solder alloy). In this homologous temperature range, the time-dependent material responses, such as creep and stress relaxation of SAC305 solder alloy, are significant, and the viscoplastic effects induced by thermal cycling are predominant. Stress relaxation tests were conducted at -55°C, 20°C and 125°C to assess the viscoplastic behavior of SAC305 solder alloy. Two test samples were considered for each configuration. A strain rate $d\varepsilon/dt = 4.8\times10^{-5}$ s^{-1} was applied until the ultimate tensile strength (UTS) was reached. The corresponding strain was then held constant for 120 minutes, and the shear stress evolution was plotted using the von Misès criteria (Figure 10). The results indicate that the relaxation rates vary with temperature. Initially, there is a sharp decrease in stress shortly after the strain is held constant, followed by a slower relaxation until reaching a saturation value 'τsat'. This initial sharp decrease in the relaxation curves becomes more pronounced as the temperature increases. Furthermore, as temperature increases, the saturation stress tends to approach zero. At the microstructural level, SAC305 solder joints consist primarily of Ag_3Sn intermetallic compounds (IMCs) embedded in a tin matrix and these IMCs act as obstacles to the movement of dislocations. To overcome these obstacles through dislocation climb and detachment processes, dislocations need to acquire sufficient energy. For instance, at -55°C, the stresses build up during the initial ramp, providing the necessary energy for dislocations to move, which results in a decrease in stress. As stress relaxation occurs, the 'source' of energy diminishes, leading to the stresses reaching a saturation value. As the temperature increases, additional thermal energy is introduced, causing the saturation stress to decrease and leading to sharper stress relaxation in the early stage of the relaxation process. To capture these effects, a double exponential law is considered:

$$\tau_{max}(t,T) = [A_1(T) - \tau_{sat}(T)]e^{-\lambda_1(T)t} + [A_2(T) - \tau_{sat}(T)]e^{-\lambda_2(T)t} + \tau_{sat}(T)$$

With τsat(T), $A_1(T)$, $A_2(T)$, $\lambda_1(T)$, and $\lambda_2(T)$ as temperature-dependent parameters. Figure 10 shows that this model accurately fits the experimental stress relaxation curves. Since the model has been developed for extreme temperatures at -55°C and 125°C, it is also possible to interpolate the model to intermediate temperatures and therefore be able to determine the stress at any given time (for t > 120 minutes, τ = τsat).

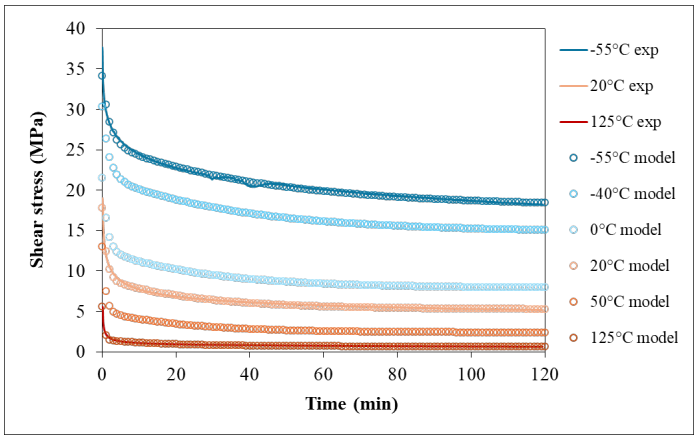

Figure 10: Mean experimental stress relaxation curves at -55°C, 20°C, and 125°C with the corresponding fitted model and interpolated curves for intermediate temperatures

This viscoplastic material characterization is important in the context of this study since it will directly be used in the calculation of the fatigue criteria of solder joints subjected to temperature cycling with dwell times, during which stress relaxation occurs.

Components

Characterizing the material properties of components is as important as characterizing the solder alloy. An approximative assessment of the Young's modulus and CTE can indeed lead to significant errors on the calculation of the fatigue criteria. In this study, a specific choice of components was made to minimize these potential errors. Mono-material components with well-known material properties were indeed selected (Table 3).

Table 3: Mechanical and thermomechanical properties of the components [15-17]

Component	Material	E (GPa)	*v*	CTE (ppm.°C^{-1})
CLCC	Al_2O_3	285	0.21	$CTE_{Al2O3}(T)$
Resistors	Al_2O_3	285	0.21	$CTE_{Al2O3}(T)$
WLP	Si	130	0.28	2.6

With $CTE_{Al2O3}(T) = 2.4\times10^{-7}\ T(°C)^3 - 5.3\times10^{-5}\ T(°C)^2 + 8.4\times10^{-3}\ T(°C) + 5.4$. For multi-material components, accurate characterization of each material (or obtaining material properties from manufacturers) is crucial for developing models to assess the overall Young's modulus and CTE of the component (see section 'Mechanical properties of the components').

Printed Circuit Boards (PCBs)

Since the model development includes a module dedicated to determining PCB material properties, it is important to characterize different laminates with various glass-fiber fabrics to calibrate the model. Dynamic Mechanical Analysis (DMA) and ThermoMechanical Analysis (TMA) were conducted to determine the Young's modulus CTE of Panasonic R1755V laminates reinforced with 1080, 2116, and 7628 glass-fiber fabrics (Figure 11 (a) and (b)).

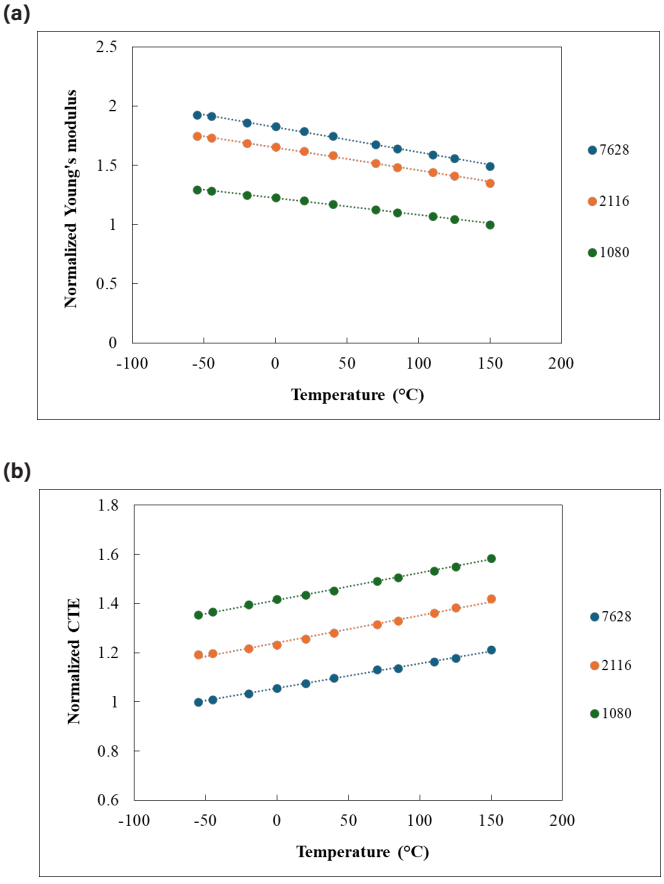

Figure 11: (a) Normalized Young's modulus and (b) CTE of the laminates as a function of the temperature

These graphs show the temperature dependency of the Young's modulus and CTE of the PCBs, which must be taken into account when assessing the durability of solder joints. In particular, the resin content in 1080, 2116 and 7628 laminates is 60%, 46%, and 46%, respectively. The Young's modulus of glass is significantly higher than that of resin, while its CTE is correspondingly lower. Moreover, the resin is more thoroughly impregnated into the glass fibers in 7628 fabrics compared to 2116 fabrics, which in turn limits its ability to expand or contract. As a result, the relative position of the curves is consistent.

DURABILITY MODEL DEVELOPMENT

Input data

Mechanical properties of the PCBs

These results were then used to calibrate the micromechanical model designed to evaluate the overall Young's modulus and coefficient of thermal expansion (CTE) of the PCBs. This model is crucial because an inaccurate assessment of these properties can lead to incorrect predictions of the electronic assembly's lifetime. The PCB stack-up structure is complex, consisting of alternating layers of copper, laminates, and cured prepregs made of epoxy resin, with varying numbers and types of glass-fiber fabrics. To evaluate the Young's modulus and CTE of a plain-woven composite (such as a prepreg or laminate material), a Representative Volume Element is considered as seen on Figure 12 [18].

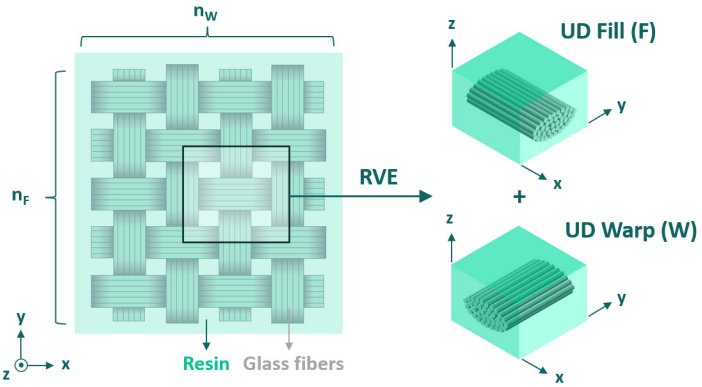

Figure 12: Schematic view of a laminate structure with its woven fabric and associated RVE

This RVE is a combination of two unidirectional elementary cells in the fill and warp directions. Based on data provided by the PCB manufacturers (resin content, yarn sections, etc.), along with the material properties of the glass fibers and resin as well as the dimensions of the RVE, a micromechanical model was developed to calculate the Young's modulus and CTE of the RVE. The calculations are primarily based on analytical laws derived from the resistance of materials and classical laminate theories, along with adjustments using experimental results. Directional Young's moduli and CTEs of the RVE are dependent on the Young's moduli and CTEs of glass and epoxy resin, along with the dimensions of the RVE. The following matrix represent the stiffness matrix of the unidirectional elementary cells (either in fill (F) or warp (W) direction):

$$\boldsymbol{C}_{F/W} = \begin{pmatrix} c_{11} = \dfrac{E_l}{1-\nu_{lt}\nu_{tl}} & c_{12} = \dfrac{\nu_{lt}E_l}{1-\nu_{lt}\nu_{tl}} & 0 \\ c_{21} = \dfrac{\nu_{tl}E_l}{1-\nu_{lt}\nu_{tl}} & c_{22} = \dfrac{E_t}{1-\nu_{lt}\nu_{tl}} & 0 \\ 0 & 0 & G_{lt} \end{pmatrix}$$

The subscripts 'l' and 't' stands for 'longitudinal' (parallel to the direction of the yarns) and 'transverse' (perpendicular to the direction of the yarns) respectively. A linear combination of the stiffness matrices of both unidirectional elementary cells allows to determine the stiffness matrix of the RVE:

$$\boldsymbol{C}_{RVE} = \frac{n_F}{n_F + n_W}\boldsymbol{C}_F + \frac{n_W}{n_F + n_W}\boldsymbol{C}_W$$

With n_f and n_w the number of yarns in the fill and warp directions respectively. The coefficients of the matrix C_{RVE} enable the determination of the directional Young's moduli of the RVE. The corresponding directional CTEs were determined using Schapery's model [19]. By considering the sandwich structure of the PCBs and the material properties of copper (E_{Cu} = 110 GPa and CTE_{Cu} = 17.10^{-6} °C^{-1}), it was then possible to assess the overall material Young's modulus and CTE of the tested PCBs (Figure 13). As shown in Figure 2, the Double-Sided (DS) PCB stack-up consists of thick glass-fiber fabrics with low resin content, in contrast to the Multi-Layer board (ML8), which is composed of glass-fiber layers of varying thicknesses and resin contents, along with copper layers. Given the mechanical and thermomechanical properties of glass, resin, and copper, the trends observed in the curves plotted in Figure 13 are consistent: $E_{ML8}(T) > E_{DS}(T)$ and $CTE_{ML8}(T) > CTE_{DS}(T)$.

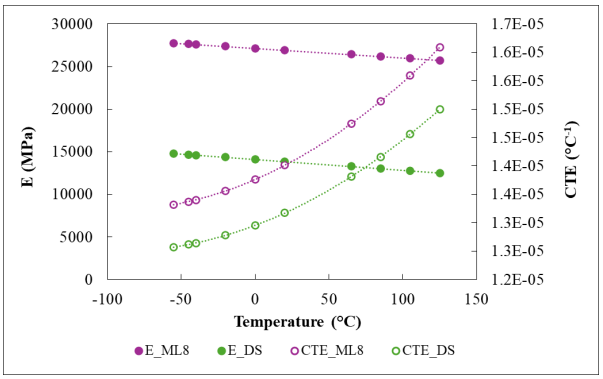

Figure 13: Temperature-dependent evolution of the Young's modulus and CTE for the DS and ML8 PCBs

As mentioned previously, determining the material properties of the PCB is a crucial step in assessing the durability of electronic assemblies. Accurately capturing the temperature-dependent evolution of the Young's modulus and CTE for any stack-up is crucial for minimizing errors in fatigue criteria calculations. The RVE model developed in this section is also useful to determine the material properties of complex components, such as BGAs.

Mechanical properties of multi-materials components (example of a BGA)

As with the PCB, determining the Young's modulus and CTE of the components soldered onto the board is also critical. There are components with 'simple' structures, such as those considered in this study (CLCC, WLP, and resistors), but there are also multi-materials components for which assessing material properties can be challenging. This is the case for components like Ball Grid Arrays (BGAs), which basically consist of a PCB substrate (generally with Bismaleimide triazine (BT) resin), a silicon die, and an encapsulant (Figure 14).

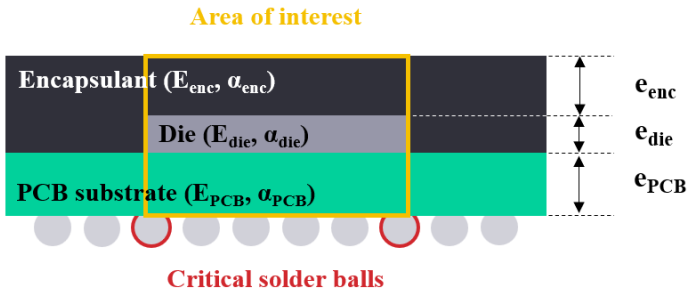

Figure 14: Simplified representation of a BGA

The area of interest is beneath the die, as experience shows that the critical solder balls subjected to thermal cycling are located at the corners underneath the die. The in-plane Young's modulus of the BGA can be approximated using the classical rule of mixtures:

$$E_{BGA}(T) = \frac{E_{PCB}(T)e_{PCB} + E_{die}e_{die} + E_{enc}(T)e_{enc}}{e_{PCB} + e_{die} + e_{enc}}$$

The subscript 'enc' is for the encapsulant material, which is generally a polymer, that is why the temperature-dependent Young's modulus must be known. The Young's modulus of the silicon die is well-established, so the challenge lies in determining the Young's modulus of the PCB substrate. By knowing the substrate's stack-up, as well as the Young's moduli of the resin and glass fibers, and applying the RVE model, it is possible to assess the Young's modulus $E_{PCB}(T)$. Regarding the CTE of the BGA, it depends on the height of the PCB substrate because the die, which has a higher Young's modulus and CTE than the PCB substrate, affects its expansion and contraction during thermal cycling (Figure 15).

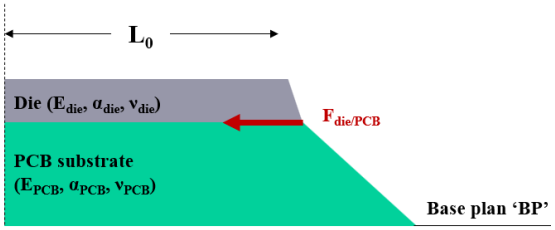

Figure 15: Local shearing of the PCB substrate during thermal cycling

Considering the shearing of the PCB during thermal cycling is important because it influences the evaluation of the CTE of the BGA at the base plane, which is in direct contact with the solder balls. The CTE of the PCB substrate's base plane is denoted 'α_{BP}' and expressed as a function of the material properties of both the PCB substrate and the die, as well as geometric data $\alpha_{BP} = f(E_{PCB}, \nu_{PCB}, e_{PCB}, E_{die}, \nu_{die}, e_{die}, L_0, \alpha_{PCB}, \alpha_{die})$. With L_0 the length of the die (assuming a square die), ν_{PCB} and ν_{die} the Poisson's ratios of the PCB substrate and the die respectively. Figure 16 shows an example of the temperature-dependent CTE of the BGA, both without and with consideration of the PCB substrate shearing.

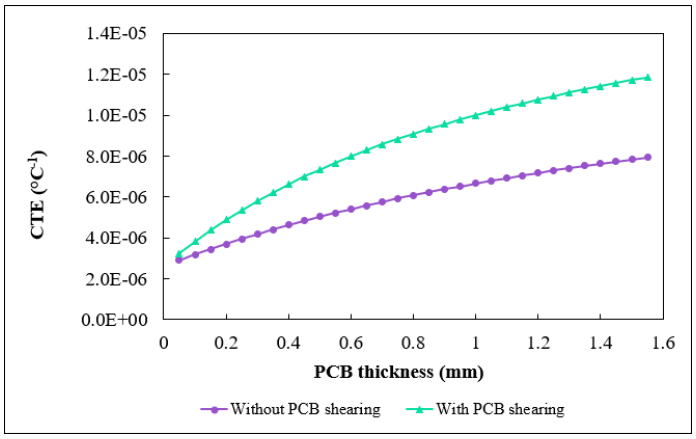

Figure 16: Evolution of the CTE of the BGA with the thickness of the PCB with and without PCB substrate shearing (die dimensions: 10 mm x 10 mm x 0.23 mm))

In this example, it is interesting to note that as the PCB substrate thickness increases, the difference between CTE of the BGA without shearing and with shearing becomes significant, indicating that considering the PCB substrate shearing is important to evaluate the CTE of the BGA. For multi-materials components, mechanical and thermomechanical characterizations are required to validate the Young's modulus and CTE models. In this study, it has been validated with three different BGAs. Characterization might still be necessary after model validation to assess the material properties of new BGA packages, as it can be challenging to obtain this information from component manufacturers.

Calculation of the fatigue criteria

Shear strain model

In this model, the assembly is assumed to be loaded in pure shear, with no bending considered. Figure 17 shows a representation of solder joint shearing during thermal cycling.

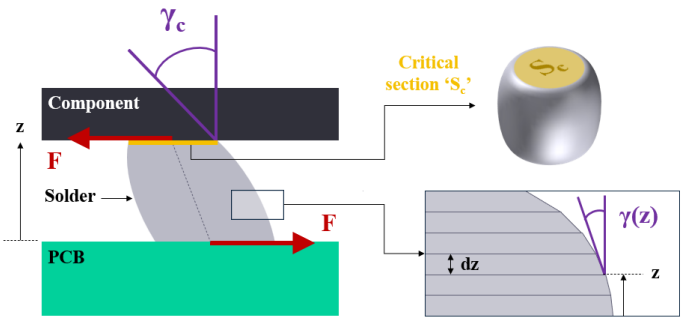

Figure 17: Shear-loaded solder joint during thermal cycling

Instead of considering a global shear angle, this model focuses on the most vulnerable part of the solder joint characterized by its critical section 'S_c'. The shear angle is indeed a function of the height 'z' and is maximum at 'S_c', which is the minimum solder joint load bearing area. The following equation gives the expression for the critical shear strain 'γc':

$$\gamma_c(t,T) = \Delta L_{max}(T) - \tau_{max}(t,T) S_c L_{eq} \left[\frac{1-\nu_p^2}{2A_p E_p(T)} + \frac{1-\nu_c}{A_c E_c(T)} \right]$$

With $\Delta L_{max}(T) = L_D . |\alpha_p(T) - \alpha_c(T)| . (T - T_{ref})$, $\tau_{max}(t,T)$ is the time and temperature-dependent maximum shear stress as depicted in Figure 10, L_D the distance between the center of the assembly and the critical solder joint, S_c the critical section of the solder joint, L_{eq} the equivalent length for array packages (for peripheral or chip-like packages, $L_{eq} = L_D$), $\alpha_p(T)$ and $\alpha_c(T)$ the temperature-dependent coefficients of thermal expansion of the PCB and the component respectively, A_p and A_c the surfaces of the PCB and component, respectively, where the forces are applied (for peripheral and array packages, $A_i = e_i.P$, where 'P' is the pitch, for chip-like components, $A_i = e_i.w$, where 'w' is the width (here, the subscript 'i' refers to either the PCB ('p') or the component ('c'))), $E_p(T)$ and $E_c(T)$, ν_p and ν_c the temperature-dependent Young's moduli and Poisson's ratios of the PCB and the component, respectively . The term 'h_i' refers to the integrated solder height, accounting for the geometry of the solder joint. This model refines the classical mathematical model by enhancing the precision of two key terms, specifically the integrated height, denoted as 'h_i', and the equivalent length, 'L_{eq}', introducing a level of precision beyond the standard formulation.

Consideration of Solder Joint Geometry

The integrated height 'h_i' is a parameter that incorporates the solder joint geometry into the model. Generally, the solder joint height, or stand-off, is included in the model, but the shape of the solder joints, whether barrel-like, sphere-like, etc., is not typically considered in analytical models. Intuitively, a cone-shaped solder joint with height 'h' would for instance fail sooner than a perfect cylindrical joint due to the reduced surface area. Figure 18 shows a schematic of a solder joint along with a reference system used to calculate the integrated height 'h_i'.

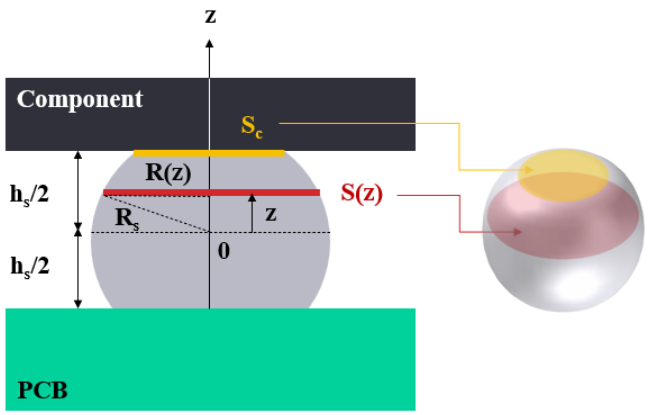

Figure 18: Schematic of a solder joint for the calculation of the integrated height 'h_i'

When moving along the z-axis, the surface area of the solder joint varies (contrary to an idealized cylindrical solder which would have a constant cross section perpendicular to the z-axis). The expression for the integrated height is as follows:

$$h_i = S_c \int_{-h_s/2}^{h_s/2} \frac{1}{S(z)} dz$$

In this specific case, $S(z) = \pi [R_s^2 - R(z)^2]$. R_s is the radius of the solder sphere and R(z) is the radius of the circular area perpendicular to the z-axis.

Effect of solder joint array

Another factor to consider when developing an analytical model is the solder array. Consider a component with peripheral solder balls spaced at a pitch 'P'. The outermost solder joint, located at a distance L_D from the center of the assembly, will experience a certain strain range 'Δγ' during thermal cycling. If we add two additional rows of solder balls spaced at the same pitch and adjacent to the original peripheral row, the strain range at the same location will change because the additional solder balls affect the forces applied to the critical solder joint. The authors demonstrated this effect in a previous study using Finite Element Modeling (FEM) [20]. Figure 19 shows the geometry of the models along with the strain range amplitudes calculated for both configurations after temperature cycles.

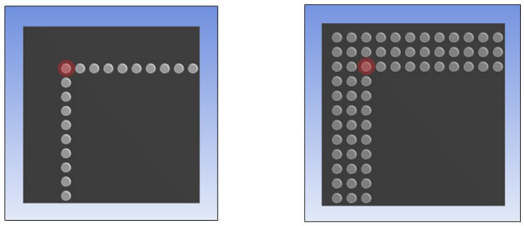

1 row $\Delta\gamma_{corner\ ball} = 1.89\times10^{-2}$

3 rows $\Delta\gamma_{corner\ ball} = 1.04\times10^{-2}$

Figure 19: Highlighting the effect of the ball grid array on the shear strain range of the corner ball in the inner row [20]

By using a unidirectional model of springs in series, it is possible to determine the equivalent length 'L_{eq}' for any type of solder array.

Model calibration

To calibrate the model, the calculation of the shear strain range was correlated to the number of cycles to failure (for a 50% failure rate) '$N_{50\%}$' measured for each component and thermal cycling conditions. The fatigue life prediction model has the following form:

$$\Delta\gamma_c = \gamma_c(t_{d,max}, T_{max}) - \gamma_c(t_{d,min}, T_{min}) = K\left[\frac{N_{50\%}}{S_c}\right]^b$$

With 'K' and 'b' representing the fatigue coefficient and exponent, respectively, which are dependent on the solder material. To account for the cracked area in each component, the number of cycles to failure '$N_{50\%}$' is scaled by the critical section 'S_c'. This technique was introduced by Clech in his tin-lead solder reliability model [21]. In this work, Clech interpreted the ratio '$N_{50\%}/S_c$' as "the number of cycles it takes for a crack, or several micro-cracks, to propagate through a unit of solder attach area". Figure 20 shows the SAC305 thermomechanical fatigue curve derived from the shear strain model and the measured number of cycles to failure ($N_{50\%}$).

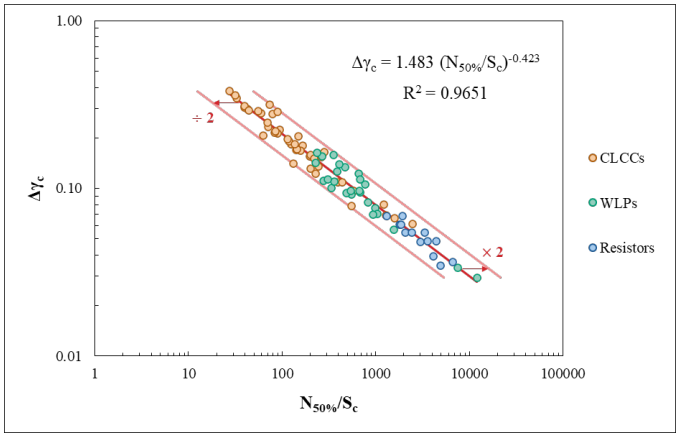

Figure 20: SAC305 thermomechanical fatigue curve

The coefficient of correlation is $R^2 = 0.9651$ and the data points fall within the [÷2, ×2] correlation band. It is interesting to notice that the fatigue exponent b = -0.423 is consistent with other fatigue models using the shear strain range as the fatigue criteria [22, 23].

Model validation

To validate this model, new sets of test vehicles subjected to different thermal cycling conditions, with different PCB stack-ups and components, including different WLPs and a BGA, were considered [24-26]. Figure 21 shows the fit of the new durability data points with the derived SAC305 reliability model. It is interesting to observe that these new durability data fit within the [÷2, ×2] correlation band. Given the inherent dispersions that exist in electronic assemblies (solder joints geometry, quality

of soldering, lot-to-lot variations, etc.), the model is reasonably accurate for assessing the durability of SAC305 solder joints subjected to temperature cycles. Additionally, the model is easy to use and can therefore be very helpful for designers and engineers involved in designing electronic equipment used in severe thermal conditions.

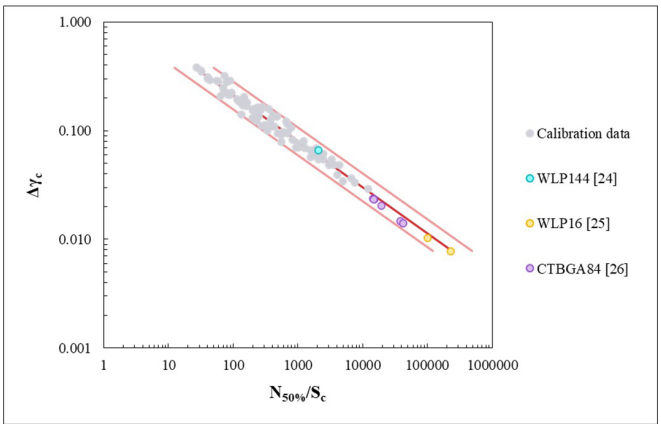

Figure 21: Comparison between the experimental validation data and the derived SAC305 reliability model

CONCLUSION

In a world where electronic system failures can result in catastrophic accidents and erode customer trust, performing reliability calculations is crucial to ensure that equipment functions reliably throughout its lifecycle. The analytical SAC305 reliability model developed in this study is designed to be practically useful for designers and reliability engineers, offering quick and accurate results without the need for Finite Element Modeling (FEM), which requires specialized skills and can be time-consuming.

The SAC305 reliability model aims to retain the simplicity of use characteristic of analytical models while enhancing certain aspects, such as the effects of array configurations in BGAs and solder joint geometry. It has been calibrated using 83 durability data points and validated with an additional 23. This model is particularly useful for common SMT components (such as BGAs, chip-like components, and CLCCs). However, when dealing with new or complex components, FEM is often necessary. In such cases, combining FEM with experimental work can be a valuable approach for capturing key effects that may eventually be incorporated into an analytical model.

Finally, the PCB material properties model discussed in this paper, while essential for assessing solder joint durability, is also practically useful for thermal analysis. The model allows for the evaluation of global density, thermal conductivity, and specific heat, which are crucial for thermal engineers conducting both steady-state and transient thermal analyses.

FUTURE WORK

The model is intended to be implemented in a software application, making it more accessible for designers and engineers. Ongoing efforts focus on integrating QFN packages and leaded components into the model. Additionally, the model could be extended to cover new Low Temperature Solder (LTS) alloys, provided comprehensive material characterization is performed.

REFERENCES

[1] J-P. Clech, R. Coyle, B. Arfaei, "Pb-Free Solder Joint Thermo-Mechanical Modeling: State of the Art and Challenges", The Journal of The Minerals, Metals & Materials Society, Advances in Electronic Interconnection Materials, Vol. 71, pp. 143-157, 2019.

[2] N. Pan, A. Henshall, F. Billaut, S. Dai, M.J. Strum, R. Lewis, E. Benedetto, J. Rayner, "An acceleration model for Sn-Ag-Cu solder joint reliability under various thermal cycle conditions", Proceedings of SMTA International, pp. 876-883, 2005.

[3] P. Lall, A. Shirgaokar, D. Arunachalam, "Norris-Landzberg acceleration factors and Goldmann constants for SAC305 lead-free electronics", Journal of Electronic Packaging, Transactions of the ASME, Vol. 134, No. 3, pp. 031008-1-031008-12, 2012.

[4] J. Miremadi, G. Henshall, A. Allen, E. Benedetto, M. Roesch, "Lead-free solder-joint reliability model enhancement", 42nd International Symposium on Microelectronics IMAPS Conference, pp. 316-323, 2009.

[5] W. Engelmaier, "Solder joints in electronics: Design for reliability", Design and Reliability of Solders and Solder Interconnections, The Minerals, Metals & Materials Society, pp. 9-19, 1997.

[6] P. Chauhan, M. Osterman, S.W. Ricky Lee, M. Pecht, "Critical review of the Engelmaier model for solder joint creep fatigue reliability", IEEE Transactions on Components and Packaging Technologies, Vol. 32, No. 3, pp. 693-700, 2009.

[7] A. Syed, "Accumulated creep strain and energy density based thermal fatigue life prediction models for SnAgCu solder joints", 54th Electronic Components and Technology Conference, Vol. 1, pp. 737-746, 2004.

[8] J-B. Libot, Z. Bussiere, P. Milesi, "Thermomechanical Durability Model of SAC305 Solder Interconnects in Wafer Level Packaging", SMTA International Conference, 2022.

[9] F. Chai, "Solder interconnect life prediction under complex temperature cycling with varying mean and amplitude", Ph.D. Dissertation, University of Maryland, 2013.

[10] IPC-9701A, "Performance test methods and qualification requirements for surface mount solder attachments", IPC standard, 2002.

[11] M. F. M. Sabri, D.A. Shnawaha, I.A. Badruddina, S. B. M. Saidb, F.X. Chec, T. Ariga, "Microstructural stability of Sn-1Ag-0.5 Cu-xAl (x= 1, 1.5, and 2wt.%) solder alloys and the effects of high-temperature aging on their mechanical properties", Materials Characterization, Vol. 78, pp. 129-143, 2013.

[12] M. Basit, M. Motalab, J.C. Suhling, P. Lall, "Viscoplastic constitutive model for lead-free solder including effects of silver content, solidification profile, and severe aging", ASME International Technical Conference and Exhibition on Packaging and Integration of Electronic and Photonic Microsystems and the ASME 13th International Conference on Nanochannels, Microchannels, and Minichannels, pp. 1-18, 2015.

[13] M.W. Xie, G. Chen, J. Yang, W.L. Xu, Temperature- and rate-dependent deformation behaviors of SAC305 solder using crystal plasticity model", Mechanics of Materials, Vol. 157, 2021.

[14] T. Sakai, A. Belakov, R. Kaibshev, H. Miura, J.J. Jonas, "Dynamic and post-dynamic recrystallization under hot, cold and severe plastic deformation conditions", Progress in Materials Science, Vol.60, pp. 130-207, 2014.

[15] L.R. Zawicki, B.W. Lenhardt, R.R. Smith, "Survivability of soldered Leadless Chip Carriers after temperature cycling", Joint American Ceramic Society (ACS) Electronics Division, pp. 1-6, 1994.

[16] P. Vianco, M.K. Neilsen, "Thermal mechanical fatigue of a 56 I/O Plastic Quad-Flat Nolead (PQFN) package", SMTA International Conference, pp. 1-10, 2015.

[17] X.J. Fan, B. Varia, Q. Han, "Design and optimization of thermo-mechanical reliability in wafer level packaging", Microelectronics Reliability, Vol.50, pp. 536-546, 2010.

[18] L. Bejan, V.F. Poterasu, "Woven composite material design by orthotropic compliance averaging method using mathematica", Computer Methods in Applied Mechanics and Engineering, Vol. 179, n° 1-2, pp. 53-65, 1999.

[19] R. Schapery, "Thermal Expansion Coefficients of Composite Materials Based on Energy Principles", Journal of Composite Materials, Vol. 2, No. 3, pp. 380-404, 1968.

[20] J-B. Libot, "Fatigue life prediction methodologies of SAC305 assemblies subjected to thermal and vibrational loading", PhD Thesis, Federal university of Toulouse Midi-Pyrénées, 2017.

[21] J-P. Clech, "Solder Reliability Solutions: A PC-based Design-for-reliability Tool", Soldering & Surface Mount Technology, Vol. 9, No. 2, pp. 45-54, 1997.

[22] W. Engelmaier, "Solder Creep-Fatigue Model Parameters for SAC & SnAg Lead-Free Solder Joint Reliability Estimation", Proceedings from IPC Midwest Conference and Exhibition, pp. 1-44, 2009.

[23] J. Mi, Y-F. Li, Y-J. Yang, W. Peng, H-Z. Huang, "Thermal Cycling Life Prediction of Sn-3.0Ag-0.5Cu Solder Joint Using Type-I Censored Data", The Scientific World Journal, Vol. 2014, No. 1, pp. 1-11, 2014.

[24] I-E. Ținca, A. Davidescu, "Analytical Fatigue Life Prediction of Ball Grid Array Solder Joints", Journal of Electronic Materials, Vol. 52, pp. 7991-8000, 2023.

[25] P-E. Tegehall, "Impact of thermal cycling profile on cracking of PCB laminate and on the fatigue life of solder joints to various types of components", RISE IVF Project Report 25357-4-O, 2019.

[26] J. Smetana, R. Coyle, E. Lundeen, I. Muntele, S. Danko, N. Hubble, B. Christian, "Board Thickness Effect on Accelerated Thermal Cycle Reliability", IPC APEX EXPO, 2021.

BIOGRAPHIES

Jean-Baptiste Libot began his career for Airbus as an Electronic Materials and Processes engineer at the Center for Advanced Life Cycle Engineering (CALCE). He then worked for more than ten years at Safran Electronics and Defense and Safran Transmission Systems in the field of electronic assembly reliability and material fatigue. He has a master's degree in Material Science, a Research Master diploma in Materials, Nanomaterials and Multi-Materials Science, and a PhD in Material science and Mechanical Engineering from the National Polytechnic Institute of Toulouse.

Philippe Milesi worked his entire career at Safran Electronics & Defense (formerly Sagem), developing a recognized expertise in the field of electronic assembly reliability throughout the aerospace and defense industry. He also has strong experience in electronic assembly-related processes. His work focuses on the development of cost-effective and easy-to-use models to assess the durability of electronic equipment. He is driven by problem solving and has a strong appetence for matching the models with experimental results. He has a bachelor's degree in mechanical engineering.